Applications of Mathematics

Kateřina Helisová; Jakub Staněk

Quermass-interaction process with convex compact grains

Applications of Mathematics, Vol. 61 (2016), No. 4, 463–487

Persistent URL: http://dml.cz/dmlcz/145796

61 (2016) APPLICATIONS OF MATHEMATICS No. 4, 463–487

QUERMASS-INTERACTION PROCESS WITH CONVEX COMPACT GRAINS

Kateřina Helisová, Jakub Staněk, Praha

(Received October 19, 2015)

Abstract. The paper concerns an extension of random disc Quermass-interaction process, i.e. the model of discs with mutual interactions, to the process of interacting objects of more general shapes. Based on the results for the random disc process and the process with polygonal grains, theoretical results for the generalized process are derived. Further, a simulation method, its advantages and the corresponding complications are described, and some examples are introduced. Finally, a short comparison to the random disc process is given.

Keywords: attractiveness; germ-grain model; Markov Chain Monte Carlo simulation; Quermass-interaction process; random set; repulsiveness; Ruelle stability

MSC 2010: 60D05, 60G55

1. Introduction

In the last years, planar random sets given by unions of objects, the so-called germ-grain models (see e.g. [2]), have been studied because of their applications in biology, material sciences, medicine, etc. Such models can describe and explain many events, e.g., the behaviour of cells in organisms (see e.g. [8]), particles in materials (see e.g. [7]) or presence of different plants (see e.g. [5]). Even when these objects are three-dimensional, we often concentrate on two-dimensional modelling, because usually, we are either interested only in the projection of the objects to the plane (e.g. ground area of plants or trees) or we study only cross-sections of a mass which create planar formations, and suppose that the behaviour of the studied object is stationary in the third dimension (e.g. organic cells or material particles).

The research was supported by Czech Science Foundation, grant No. 13-05466P.

The basic model of such a random set is the Boolean model described theoretically e.g. in [11]. It is the random set given by the union of compact sets whose positions and shapes are independent of each other. Its special type—the random disc Boolean model, i.e., the Boolean model formed by the union of discs without any interaction—is very popular. Examples of its applications to real data can be found e.g. in [5] or [15]. However, as shown in both the publications mentioned, this model is not suitable for many situations. For example in [5], where presence of heather bushes is studied, it is realized that in the data image, the plants are more connected than the discs in realizations of the fitted Boolean model. In [15], where tumour cells are modelled, the authors apply the random disc Boolean model even when some of the cells in the data are not circular. Both these situations show that extensions of this model may be useful.

One extension consists in adding some interactions among the discs. This topic is quite well explored. For example in [9], the Quermass-interaction process is studied. In the finite case, it is the model from an exponential family, where the canonical sufficient statistic is given by Minkowski functionals of the union of discs within a bounded observation window. In [3], the proof of existence of a stationary Quermass-interaction model in $\mathbb{R}^2$ is given. The authors of [9] provide many theoretical results for this model, too, however, a discussion of simulations and statistical inference methods are missing in this paper, possibly because such methods are computationally difficult. The Quermass-interaction model is extended, theoretically analyzed and simulated by Markov Chain Monte Carlo method (MCMC), namely by birth-death Metropolis-Hastings algorithm, in [12]. Maximum likelihood-based inference using MCMC techniques (MCMC MLE, see [14]) for this process are discussed in [13]. Further procedures of statistical inference for this model are established in [20], where the dimension of the model is reduced by the classical principal component method in order to make the estimating method faster, and in [4], where the authors apply Takacs-Fiksel procedure which allows to estimate the intensity of the process. Further in [21] and [22], the random disc Boolean model is extended by considering its time evolution, and other statistical methods for estimating the parameters, namely particle filter and MCMC particle filter, are applied and compared to MCMC MLE.

Another extension of the random disc Boolean model is given by considering differently shaped grains instead of discs. Such a model is not well explored. In [9], the authors derive some theoretical results for the Quermass-interaction process with non circular grains. They focus mainly on stability properties while simulation and statistical inference procedures are not studied.

In this paper, we consider also the Quermass-interaction process with grains which may be non circular. The paper is organized as follows. In Section 2, we describe the

model. Then in Section 3, we derive some theoretical results, which are not mentioned in [9]. Particularly, we focus on Ruelle stability, while we correct the conditions introduced in [9] for a special type of the process, the so-called χ-interaction process, with polygonal grains in order for it to be Ruelle stable, and then we formulate conditions for the process with grains having smooth border and some other special properties in order for it to be Ruelle stable, too. Further, we define conditions for attractiveness and repulsiveness of the process, which are important for simulations since they control the behaviour of the simulated realizations. Section 4 concerns the simulation procedure of the process. Here, we mention various possibilities and discuss their advantages and disadvantages, and we show some examples. All plots in this section are produced by R (see [19]). At the end of Section 4, we provide a short comparison to the simulation method introduced in [12] developed for the random disc model.

2. Model description

The Quermass-interaction process is a random planar set which belongs to the class of random sets called germ-grain models (see [2]). These sets are given by the union of objects with random shapes (so-called grains) which are randomly scattered in the plane and their locations are given by reference points (so-called germs).

More precisely, consider a planar geometrical object $x = u + x_0$ with reference point $u \in \mathbb{R}^2$ (germ) and shape $x_0 \subset \mathbb{R}^2$ (grain) which is a realization of a random planar convex compact set $\mathbf{X}$ (so-called typical grain) with distribution Q. Denote by $\mathbf{x} = \{x_1, \dots, x_n\}$ a finite configuration of n such geometrical objects and by $U_{\mathbf{x}}$ the union of the objects from the configuration $\mathbf{x}$.

Further, consider a Boolean model $\mathbf{Y}$ (i.e. the germ-grain model whose germs form a Poisson process, the grains are independent identically distributed, and their distribution is independent of the distribution of the germs) with an intensity function of the germs $\varrho(u) = \varrho > 0$ on a bounded set $S \subset \mathbb{R}^2$ and $\varrho(u) = 0$ otherwise, with the distributions of its grains given by the distribution of $\mathbf{X}$.

Then consider a random set $\mathbf{Z}$ which is absolutely continuous with respect to the process $\mathbf{Y}$, its realizations are formed by unions of finite configurations $\mathbf{x} = \{x_1, \dots, x_n\}$ of the objects $x_1, \dots, x_n$, and the set $\mathbf{Z}$ is described by a density $f_\theta(\mathbf{x})$ with respect to the probability measure of $\mathbf{Y}$.

The Quermass-interaction process with convex compact grains is the random set $\mathbf{Z}$ whose density with respect to $\mathbf{Y}$ is of the form

$$f_{\boldsymbol{\theta}}(\mathbf{x}) = c_{\boldsymbol{\theta}}^{-1} \exp\{\theta_1 A(U_{\mathbf{x}}) + \theta_2 L(U_{\mathbf{x}}) + \theta_3 \chi(U_{\mathbf{x}})\}, \tag{2.1}$$

where $A(U_{\mathbf{x}})$ is the total area, $L(U_{\mathbf{x}})$ the perimeter and $\chi(U_{\mathbf{x}})$ the Euler-Poincaré characteristic (the number of connected components minus the number of holes) of the union $U_{\mathbf{x}}$, $\theta = (\theta_1, \theta_2, \theta_3)$ is a vector of parameters, and c_θ is a normalizing constant.

The interpretation of the parameters θ_i, $i = 1, 2, 3$, is such that positive values of θ_i force the process to produce realizations with larger i-th characteristic comparing to the reference process while the realizations from the density with negative θ_i have the i-th characteristic mostly smaller. Note that the process with $\theta_1 = \theta_2 = \theta_3 = 0$ is the reference Boolean model.

3. Theoretical properties

In [9], the authors study in detail the random disc Quermass-interaction process (i.e. the process defined above, where the typical grain $\mathbf{X}$ is a disc with random radius) and the process with polygonal grains, and provide the first theoretical results. Later in [12] and [13], random disc Quermass-interaction process is extended by considering more geometrical characteristics, e.g. the number of isolated discs, or the number of connected components and the number of holes considered separately. In addition to some new theoretical results, these two papers describe also simulations and statistical analysis, respectively. All these studies form the base for the research in this paper.

The results presented in this section are mainly based on geometrical characteristics of the objects or their parts. Therefore, let us first define two basic terms used often in the sequel.

Let $\mathbf{Z}$ be a (random) planar set. Then the hole of the set $\mathbf{Z}$ is an open bounded planar set h such that for all $u \in h$ we have that $u \notin \mathbf{Z}$, and the boundary of its closure $\bar{h}$ is a part of the boundary of $\mathbf{Z}$, i.e. $\partial\bar{h} \subset \partial\mathbf{Z}$.

Assume that $\mathbf{Z} = \bigcup_{i=1}^{n} x_i$, x_i are convex compact sets (grains). By a vertex of the hole h we mean a point $v \in \partial\bar{h}$ such that there exist two grains x_i and x_j satisfying $v \in \partial x_i \cap \partial x_j$.

3.1. Measurability and integrability of the density. The first theoretical question is whether the Quermass-interaction process given by (2.1) is well defined, i.e. whether the density $f_{\boldsymbol{\theta}}$ is measurable and integrable.

Following the definition of the Quermass-interaction process in [9], denote by $W_j^2(\cdot)$, $j = 0, 1, 2$, the Minkowski functionals (Quermass integrals) in $\mathbb{R}^2$. Due to the fact that $(A(U_{\mathbf{x}}), L(U_{\mathbf{x}}), \chi(U_{\mathbf{x}})) = (W_0^2(U_{\mathbf{x}}), 2W_1^2(U_{\mathbf{x}}), W_2^2(U_{\mathbf{x}})/\pi)$, the results

for the general model from [9] hold for our model as well. Hence, the measurability of density $f_{\boldsymbol{\theta}}$ follows directly from Lemma 2.2 in [9].

Further, we focus on the Ruelle stability of the process, since it is a sufficient condition for integrability of the density $f_{\boldsymbol{\theta}}$ (see [9]). The density $f_{\boldsymbol{\theta}}$ is called to be Ruelle stable if there exist positive constants α and β such that $f_{\boldsymbol{\theta}}(\mathbf{x}) \leqslant \alpha\beta^{n(\mathbf{x})}$ holds for all configurations $\mathbf{x}$, where $n(\mathbf{x})$ denotes the number of objects x_i in the configuration $\mathbf{x}$. Hence, the stability condition holds if and only if the energy

$$E(\mathbf{x}) = -\log\Big(\frac{f_{\boldsymbol{\theta}}(\mathbf{x})}{f_{\boldsymbol{\theta}}(\emptyset)}\Big)$$

is bounded below by a bound which is linear with respect to the number of points $n(\mathbf{x})$, i.e.

$$E(\mathbf{x}) \geqslant -A - Bn(\mathbf{x})$$

holds for some positive constants A and B.

In the following proposition, we reformulate the results from [9] for our model. While the reformulations of the first two parts are straightforward, the last part uses conditions different from the ones introduced in [9], and so it requires more detailed discussion.

Proposition 3.1. (1) *Consider the (A, L)-interaction process, i.e. the Quermass-interaction process with the density $f_{\boldsymbol{\theta}}$ given by*

$$f_{\boldsymbol{\theta}}(\mathbf{x}) = c_{\boldsymbol{\theta}}^{-1} \exp\{\theta_1 A(U_{\mathbf{x}}) + \theta_2 L(U_{\mathbf{x}})\}.$$

Then the density $f_{\boldsymbol{\theta}}$ is Ruelle stable if one of the following conditions holds:

(a) $\theta_1 \leqslant 0$ *and* $\theta_2 \leqslant 0$,

(b) $\theta_1 > 0$, $\theta_2 > 0$, *and $A(x)$ and $L(x)$ are bounded above for all x in the support of the distribution Q of $\mathbf{X}$.*

(2) *Consider the χ-interaction process, i.e. the Quermass-interaction process with the density $f_{\boldsymbol{\theta}}$ given by*

$$f_{\boldsymbol{\theta}}(\mathbf{x}) = c_{\boldsymbol{\theta}}^{-1} \exp\{\theta_3 \chi(U_{\mathbf{x}})\},$$

whose grains are random discs. Then the density $f_{\boldsymbol{\theta}}$ is Ruelle stable for all $\theta_3 \in \mathbb{R}$.

(3) *Consider the χ-interaction process, i.e. the Quermass-interaction process with the density $f_{\boldsymbol{\theta}}$ given by*

$$f_{\boldsymbol{\theta}}(\mathbf{x}) = c_{\boldsymbol{\theta}}^{-1} \exp\{\theta_3 \chi(U_{\mathbf{x}})\},$$

whose grains are random polygons $\mathbf{X}$ satisfying the following conditions:

(a) *There exist an angle $\varphi > 0$ and radius $r > 0$ such that for all realizations x and all vertices v_x of x, the intersection $b(v_x, r) \cap \mathbf{x}$ is a circular sector of angle at least φ, where $b(v, r)$ is a disc with centre at v and radius r.*

(b) *There exists a constant $K \in \mathbb{R}$ such that $x \subset [-K, K]^2$ for all realizations x.*

Then the density $f_{\boldsymbol{\theta}}$ is Ruelle stable.

P r o o f. The major part of the proof of this proposition can be found in [9], however there are some points which require comments and corrections. Therefore, let us give here a few remarks to the proof:

(1) The first part of the proposition follows directly from Lemma 2.3 in [9] and the fact that $\overline{W}_j^2(\cdot) = W_j^2(\cdot)$ for $j = 0, 1$, where $\overline{W}_j^2$ denote the positive extension of the Minkowski functional used in the mentioned lemma.

(2) This part is the straightforward reformulation of Corollary 4.4 in [9].

(3) This part follows from Theorem 5.2 in [9] which introduces a sufficient condition for Euler-Poincaré characteristic to be bounded above and below by $C_1 n(\mathbf{x})$ and $C_2 n(\mathbf{x})$, respectively, where C_1 and C_2 are constants. The theorem is formulated for grains x satisfying the so-called uniform wedge condition of angle $\varphi > 0$ and radius $r > 0$, which means that for any point $y \in \partial x$, the intersection $b(y, r) \cap x$ is a circular sector. In part A of the proof of Theorem 5.2 in [9], it is shown that it is a sufficient condition for bounding the number of holes in $U_{\mathbf{x}}$. In part B, where the uniform wedge condition is used, it is shown that it is enough to consider the case where grains are infinite convex random planar wedges of angle at least φ.

However, no polygon satisfies the uniform wedge condition as defined in [9]. Therefore, we formulate new conditions (a) and (b) which give us the same result and allow us to follow the idea of the original proof. Condition (b) together with boundedness of S ensure that $U_{\mathbf{x}}$ lies in a bounded window $S \oplus [-K, K]^2$ which can be covered by a finite number of discs with radius $r/2$. Hence it suffices to show that the number of holes of $U_{\mathbf{x}}$ lying in arbitrary disc with radius $r/2$ is bounded above by $C_3 n(\mathbf{x})$, where C_3 is a constant. Finally, as each admissible polygon has no more than one vertex in each disc with such radius, we can focus only on the case where grains are infinite convex random planar wedges of angle at least φ.

The remaining part of the proof is identical to the one introduced in [9].

Note that the condition (b) in part (3) is required, even if it is not used in the original result. Only boundedness of S is not sufficient, because the counterexample presented in [9] can be interpreted as shown in Fig. 1. There are two realizations of germ-grain process with polygonal grains where in the first case, the germs form the centres of gravity, while in the second case, the germs may lie outside the interior of the grains. In general, we can assume an arbitrary distribution of the distance of the grains from their germs. Then although the germs are scattered in the same

bounded window S, the grains may be arbitrarily far from the germs. Therefore, the lower limit for the length of the side of the polygon, which is in [9] considered to be a sufficient condition for keeping the Ruelle stability, is irrelevant because a shift of the grains further from their germs has the same effect as shrinking the length side (in the sense that we can enlarge the number of sides of the polygon even when the lengths of the sides are the same). Thus, as introduced in [9] and shown in Fig. 1, n polygons may build configurations with $O(n^2)$ holes, so there is no linear boundedness of the number of holes with respect to the number of grains. □

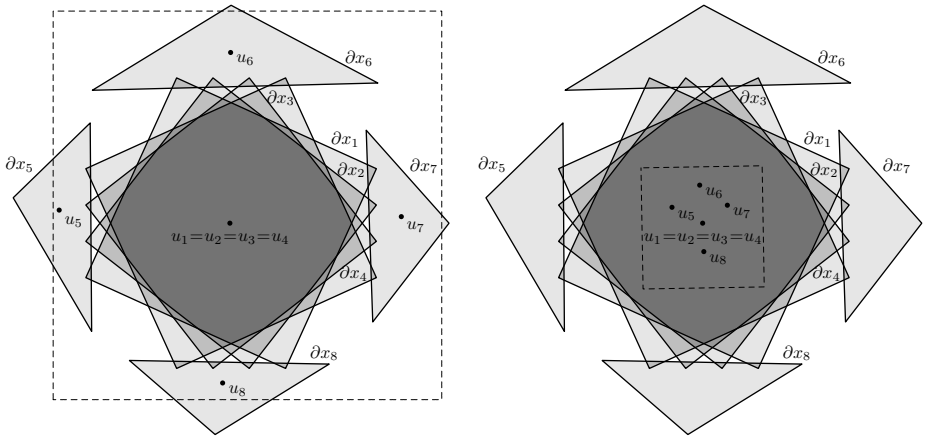

Figure 1. Two realizations of the germ-grain model with polygonal grains, where germs are scattered in the same bounded window S, where in the left figure, the germs form the centres of gravity, while in the right figure, the germs may lie outside the grains.

Recall that the introduced proposition mentioned Ruelle stability for A-interaction and L-interaction process with general convex compact grains, and for χ-interaction process of discs or polygons. In the following paragraphs, we formulate a new result describing the conditions for Ruelle stability of χ-interaction process with another shape of grains. Namely, we focus on grains having smooth boundary with bounded curvature such as ellipses with bounded ratios of the main axes, several ovoid shapes etc. More precisely, we will consider convex compact grains x satisfying the following conditions:

(1) There exists a constant $K > 0$ such that $x \subset [-K, K]^2$.
(2) For each x, we have $\partial x \in C^1$, i.e. there exists a tangent of the grain at each point on its boundary.
(3) Denote by T_v^x, T_w^x the tangents of ∂x at the points $v, w \in \partial x$ and by $\alpha_{v,w}^x$ the smaller angle between T_v^x and T_w^x. Then there exists a constant L such that

$$\alpha_{v,w}^x \leqslant L\|v - w\|.$$

Just note that for grains x such that $\partial x \in C^2$ it means that the curvature of ∂x is bounded.

(4) There exists $\tilde{r} > 0$ such that any two grains x_i, x_j, $i \neq j$, satisfy

$$\sharp(\partial x_i \cap \partial x_j \cap b(u, \tilde{r})) \leqslant 2 \quad \forall\, u \in \mathbb{R}^2,$$

i.e. that the boundaries of arbitrary grains have at most two intersections in an arbitrary disc with radius $\tilde{r}$.

Note that the assumptions (1)–(3) are not very restrictive while the assumption (4) is stronger. However, there exist shapes satisfying these conditions, e.g. the ellipses with bounded ratios of the axes as mentioned above having moreover limited orientation.

Further note that all the assumptions (1)–(4) may be satisfied also by some non-convex grains, but the following proposition holds only for the convex compact ones.

Proposition 3.2. *Every χ-interaction process with convex compact grains satisfying the above conditions* (1)–(4) *is Ruelle stable.*

To prove this proposition, we need the following lemma.

Lemma 3.1. *Let $b(u, r)$ be a ball with the centre $u \in \mathbb{R}^2$ and the radius $r \leqslant \pi/24L$, and let h be an arbitrary hole of $U_{\mathbf{x}}$. Denote by*

$$S_h = \{v \in \partial h\colon\ i, j \in I \text{ (index set)},\ i \neq j,\ v \in \partial x_i \cap \partial x_j \cap b(u, r)\}$$

the set of all vertices of the hole h lying in the ball $b(u, r)$. Further, for each $v \in S_h$, denote by α_v the angle between the tangents $T_v^{x_i}$ and $T_v^{x_j}$, where $v \in \partial x_i \cap \partial x_j$.

Then for each $v \in S_h$ there are at most two angles α_v such that $\alpha_v < \pi/6$.

P r o o f. Note that $r \leqslant \pi/(24L)$ implies that $\alpha_{u,v}^{x_i} \leqslant \pi/12$ for all $u, v \in S_h$.

Hence, if we denote by V_v^h the wedge of the angle $\alpha_v + \pi/6$ with the vertex v and the bisector coinciding with the bisector of the angle α_v, where the wedge V_v^h is pointing into the hole h (see Fig. 2), then $h \cap b(u, r) \subset V_v^h \cap b(u, r)$.

For a fixed hole h, consider the vertices v_i, $i = 1, 2, 3$, such that $\alpha_{v_i} < \pi/6$. Then the triangle given by these three vertices has to be a subset of $V_{v_i}^h \cap b(u, r)$, because $h \cap b(u, r) \subset V_{v_i}^h \cap b(u, r)$ and $v_i \in \partial h$. Denoting by β_{v_i}, $i = 1, 2, 3$, the angles of the triangle, then $\beta_{v_i} \leqslant \alpha_{v_i} + \pi/6$, and so we get

$$\pi = \sum_{i=1}^{3} \beta_{v_i} \leqslant \sum_{i=1}^{3} \alpha_{v_i} + \pi/2 < \pi.$$

Therefore, there cannot exist three angles α_{v_i}, $i = 1, 2, 3$, such that $\alpha_{v_i} < \pi/6$. □

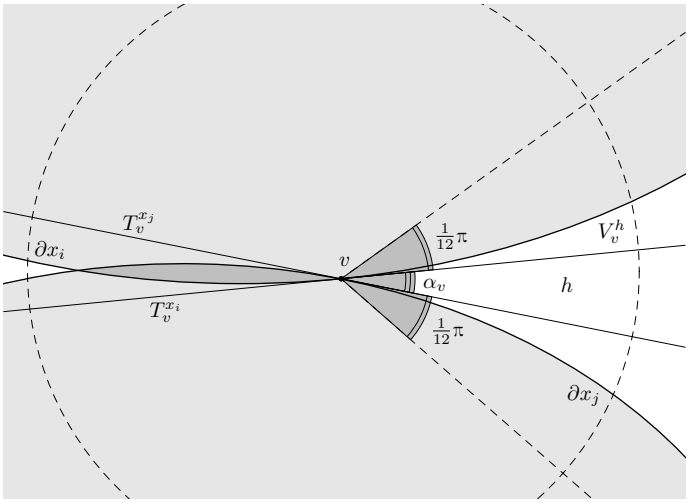

Figure 2. The disc $b(u,r)$ (circular dashed line), two grains x_i and x_j with their boundaries ∂x_i and ∂x_j (solid line), one of their intersections, the point v, being one of the vertices of the hole h, the corresponding angle α_v and wedge V_v^h, and the sector of the angle $\alpha_v + \pi/6$ (straight dashed lines) forming the restriction for the placement of the hole h.

Now let us prove the proposition.

P r o o f. From the definition of Ruelle stability, it is clear that we need to find linear boundaries for $\chi(U_{\mathbf{x}})$, i.e. constants K_1, K_2, K_3, and K_4 such that all realizations $\mathbf{x}$, satisfy

$$K_1 n(\mathbf{x}) + K_2 \leqslant \chi(U_{\mathbf{x}}) \leqslant K_3 n(\mathbf{x}) + K_4.$$

Since $\chi(U_{\mathbf{x}}) = N_{\mathrm{cc}}(U_{\mathbf{x}}) - N_{\mathrm{h}}(U_{\mathbf{x}})$, where N_{cc} denotes the number of connected components and N_{h} the number of holes, and $N_{\mathrm{cc}}(U_{\mathbf{x}}) \leqslant n(\mathbf{x})$, where $n(\mathbf{x})$ is the (finite) number of grains, we only need to prove that $N_{\mathrm{h}}(U_{\mathbf{x}}) \leqslant K_5 n(\mathbf{x}) + K_6$.

The structure of the proof is the following:

(1) We focus on a specific part of the observation window given by a ball (denoted as $b(u,r)$) with specific radius, and show that it is enough to bound the number of holes in this ball.

(2) Using Lemma 3.1, we show that for each hole h, there exist at most two wedges, denoted as $V_v^{h^c}$ and $V_w^{h^c}$, such that each other hole h' lying (at least partially) in the ball $b(u,r)$ is contained in $V_v^{h^c}$ or $V_w^{h^c}$, i.e. $(h' \cap b(u,r)) \subset (V_v^{h^c} \cup V_w^{h^c})$.

(3) Based on the step (2), we order the holes lying in the ball $b(u,r)$ to a sequence.

(4) We show that we can uniquely select two vertices from each hole and order them, so we can form the corresponding sequence of such vertices.

(5) The sequence of the vertices uniquely divides the group of the grains forming holes into two parts which form sequences $\{a_m\}$ and $\{b_m\}$. We can uniquely

form their subsequences $\{\hat{a}_m\}$ and $\{\hat{b}_m\}$ (so that the elements repeated adjacently in the sequences $\{a_m\}$ and $\{b_m\}$ are represented only once) with the property that the number of elements in the larger one is bounded below.

(6) We prove that $\{\hat{a}_m\}$ and $\{\hat{b}_m\}$ satisfy the conditions of the Davenport-Schinzel sequence of the order s (see [10]).

(7) The properties of the Davenport-Schinzel sequence are used to prove that the numbers of elements in $\{\hat{a}_m\}$ and $\{\hat{b}_m\}$ are bounded, and thus the number of holes in the considered ball must be bounded, too.

Now let us go through the proof step by step in details:

(1) Denote

$$r = \min\Big\{\tilde{r}, \frac{\pi}{24L}\Big\},$$

where $\tilde{r}$ is defined above by the property (4) of the grains. From the property (1) of the grains, we know that the whole union $U_{\mathbf{x}}$ lies in a bounded window $S \oplus [-K, K]^2$ which can be covered by a finite number of discs with radius r. Therefore, it is enough to prove that the number of holes in an arbitrary disc $b(u, r)$ with radius r is bounded above, where the hole h is considered to lie in the disc $b(u, r)$ if $A(h \cap b(u, r)) > 0$, which means that we count also the holes which are only partially obtained in the considered disc.

The chosen r ensures that

- ▷ for arbitrary grains x_i and x_j, there are at most two intersections $\partial x_i \cap \partial x_j$ of their boundaries (property (4) of the grains),
- ▷ for any grain x and arbitrary points $v, w \in \partial x \cap b(u, r)$, the angle α between the tangents T_v^x and T_w^x is less then or equal to $\pi/12$ (property (3) of the grains).

(2) Consider now the disc $b(u, r)$ for the given u and r defined above, and let h be a hole of $U_{\mathbf{x}}$ such that $A(h \cap b(u, r)) > 0$. Let $v \in S_h$ be the vertex formed by the grains x_i and x_j. If $\alpha_v < \pi/6$, denote by $V_v^{h^c}$ the wedge of the angle $\pi/6 - \alpha_v$ with vertex v and the bisector coinciding with the bisector of the angle α_v but pointing out of the hole h (see Fig. 3 (a)). Further, denote by $V_v^{x_i}$ the wedge of the angle $5\pi/6$ with vertex v, the bisector given by the normal vector with respect to $T_v^{x_i}$ and pointed into the set x_i (see Fig. 3 (a), too).

Since for arbitrary points $v, w \in \partial x_i \cap b(u, r)$, the maximal angle between the tangents $T_v^{x_i}$ and $T_w^{x_i}$ is $\pi/12$ (see the first step of this proof), ∂x_i cannot cross the boundary of the wedge $V_v^{x_i}$ in the ball $b(u, r)$. Thus, $V_v^{x_i} \cap b(u, r) \subset x_i$, and so for an arbitrary hole h' of $U_{\mathbf{x}}$, we have $h' \cap b(u, r) \subset (V_v^h \cup V_v^{h^c}) \cap b(u, r)$. As only h can be in $\bigcap_{v \in S_h} V_v^h$, hence for an arbitrary hole $h' \neq h$ we have $h' \cap b(u, r) \subset \bigcup_{v \in S_h} V_v^{h^c}$. From Lemma 3.1 we know that there are at most two vertices $v_1, v_2 \in S_h$ such that $V_{v_1}^{h^c} \neq \emptyset$ and $V_{v_2}^{h^c} \neq \emptyset$.

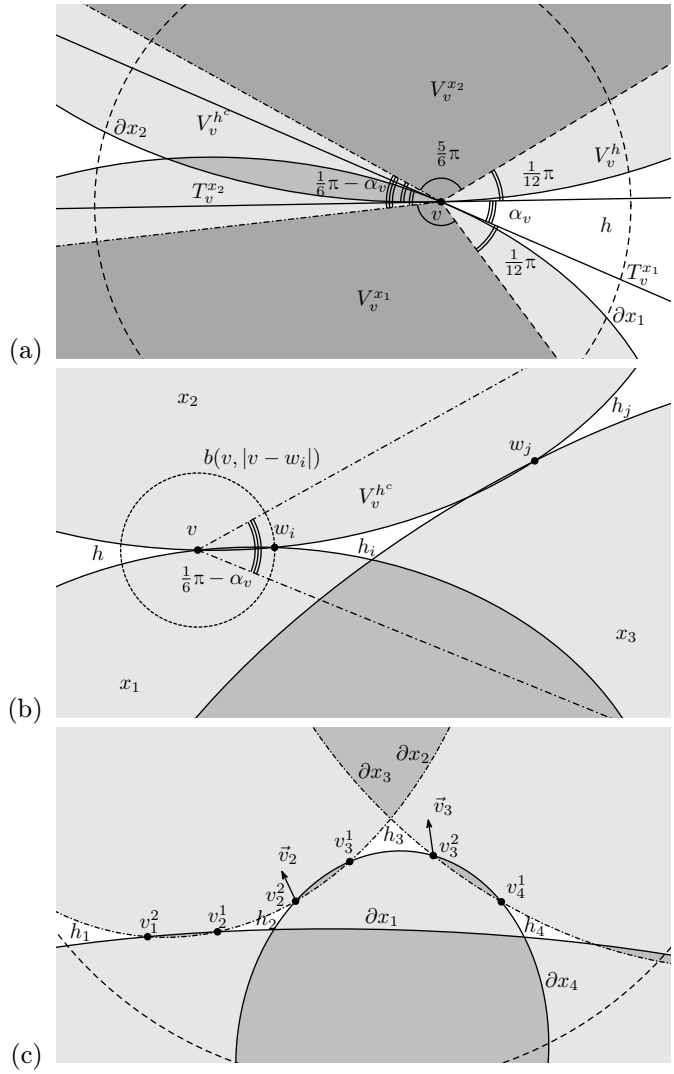

Figure 3. In (a) and (c), the disc $b(u, r)$ is denoted by dashed line. Figure (a), illustrates two grains with their boundaries (solid line), the corresponding angles, their wedges and boundedness. Figure (b) shows that the distance of two vertices of holes in the disc $b(u, r)$ is unique. Figure (c) illustrates an example of holes with the corresponding vertices v_k^1 and v_k^2, vectors $\vec{v}_k$, while the grain boundaries are denoted by solid or dot-dashed lines according to their position with respect to the direction of $\vec{v}_k$. The sequences $\{a_m\}$, $\{b_m\}$, $\{\hat{a}_m\}$ and $\{\hat{b}_m\}$ are $\{a_m\} = \{x_2, x_2, x_2, x_3\}$, $\{b_m\} = \{x_1, x_4, x_4, x_4\}$, $\{\hat{a}_m\} = \{x_2, x_3\}$ and $\{\hat{b}_m\} = \{x_1, x_4\}$. (Just note that for greater clarity, the curvature of the grains in this figure is larger than allows the property (3) of the grains and the angles do not correspond to the introduced values. However, in the real case, the holes would be too flat so the graphical illustration would not be apt enough.)

(3) Now suppose $N > 2$ is the number of holes in $b(u, r)$.

First, we show that the distance between the holes is given by the distance between their vertices v such that $\alpha_v < \pi/6$. Denote $\tilde{h} = h \cap b(u, r)$ and assume that $\tilde{h} \neq \emptyset$. Consider $v \in S_h$ with $\alpha_v < \pi/6$. Then the angles of both the wedges V_v^h and $V_v^{h^c}$ are less than $\pi/2$. Therefore, for all $x \in V_v^{h^c}$ we have $d(x, V_v^h) = \inf_{y \in V_v^h} d(x, y) = d(x, v)$ and analogously, for all $y \in V_v^h$ we have $d(y, V_v^{h^c}) = d(y, v)$ (see Fig. 3 (a)). Now consider a hole $h_j \subset V_v^{h^c}$. From the above it follows that if $v \in S_h$, $w \in S_{h_j}$, $\tilde{h} \subset V_w^{h_j^c}$ and $\tilde{h}_j \subset V_v^{h^c}$, then $d(\tilde{h}, \tilde{h}_j) = d(v, w)$.

Secondly, we show that for a hole h such that $\tilde{h}$ is nonempty, there cannot exist two holes h_i and h_j lying in the same wedge $V_v^{h^c}$ and having nonempty $\tilde{h}_i$ and $\tilde{h}_j$, respectively, so that $d(\tilde{h}, \tilde{h}_i) = d(\tilde{h}, \tilde{h}_j)$. Denote by w_i and w_j the vertices of $\tilde{h}_i$ and $\tilde{h}_j$, respectively, so that $d(\tilde{h}, \tilde{h}_i) = d(\tilde{h}, w_i)$ and $d(\tilde{h}, \tilde{h}_j) = d(\tilde{h}, w_j)$. If we suppose that $d(\tilde{h}, \tilde{h}_i) = d(\tilde{h}, \tilde{h}_j)$, then w_j lies on the circle $\partial b(v, |v - w_i|)$. But due to the bounded curvature of the grains, no other vertex of a hole can lie on this circle in $V_v^{h^c}$, because $\partial b(v, |v - w_i|) \cap V_v^{h^c} \subset x_k \cup x_l$, where x_k and x_l are the grains for which $w_i \in \partial x_k \cup \partial x_l$. Thus the hole h_i with $d(\tilde{h}, \tilde{h}_i) = \min_j d(\tilde{h}, \tilde{h}_j)$ is unique in $V_v^{h^c}$ (see Fig. 3 (b)).

Thus, we can form a sequence $\{h_1, h_2, \ldots, h_N\}$ of all holes lying in $b(u, r)$ so that h_k, $k = 2, \ldots, N-1$, have exactly two vertices v_k^1, v_k^2 such that $\alpha_{v_k^1} < \pi/6$, $\alpha_{v_k^2} < \pi/6$ and $d(h_k, h_{k+1}) = d(v_k^2, v_{k+1}^1) < d(h_k, h_l)$ for all $l > k+1$. We do it so that we choose an arbitrary hole with two vertices v_k^1, v_k^2 such that $\alpha_{v_k^1} < \pi/6$ and $\alpha_{v_k^2} < \pi/6$ (there must exist such a hole because $N > 2$), and denote it h_k, $k \in \mathbb{Z}$ arbitrary. We know that all holes in $b(u, r)$ must lie in $V_{v_k^1}^{h^c} \cup V_{v_k^2}^{h^c}$. So without loss of generality, denote the closest hole lying in $V_{v_k^1}^{h^c}$ as h_{k-1} and the closest hole lying in $V_{v_k^2}^{h^c}$ as h_{k+1}. Repeat the procedure for h_{k-1} and h_{k+1} and then for further holes in the sequence until there are no non-indexed holes with two vertices with $\alpha < \pi/6$. If there are no such holes, then the holes in $b(u, r)$ (including the ones with one vertex with $\alpha < \pi/6$ if there are some) have N consecutive indices, so it remains to shift the indices of the holes in order to obtain $\{h_1, h_2, \ldots, h_N\}$.

(4) According to the above, we can form the sequence of vertices $\{v_2^1, v_2^2, v_3^1, v_3^2, \ldots v_{N-1}^1, v_{N-1}^2\}$. For each couple of vertices v_i^1, v_i^2, denote

$$\vec{v_i} = (v_i^2 - v_i^1) \begin{pmatrix} 0 & -1 \\ 1 & 0 \end{pmatrix}.$$

Its usage is the following. We say that the grain x lies in the direction $\vec{v}$ from the vertex v iff there exists $\varepsilon > 0$ such that $v + \varepsilon \vec{v} \in x$. Then each of the vertices v_k^l, $l = 1, 2$, is given by the intersection of two grains such that one of the grains lies in

the direction $\vec{v}_k$ from the vertex v_k^l and the other lies in the opposite direction (see Fig. 3 (c)).

(5) Recall that we have the sequence $\{v_2^1, \dots, v_{N-1}^2\}$ of $2N-4$ vertices. To each vertex v in the sequence, we can assign a uniquely defined vector $\vec{v}$ (so that to the vertex v_k^l, $l = 1, 2$, the $\vec{v}_k$ is assigned for all $k = 2, \dots, N-1$). Each vertex v is an intersection of two grains, where one of them lies in the direction $\vec{v}$ from v and the other lies in the opposite direction, so we can construct two corresponding sequences of grains, the first lying in the directions of the vectors $\vec{v}$ and the other formed by the grains lying in the opposite directions.

Denote these sequences as $\{a_m\}_{m=1}^{2N-4}$ and $\{b_m\}_{m=1}^{2N-4}$, respectively. Since for all $k = 1, \dots, N-2$, v_k^1 and v_k^2 cannot be formed by the same couple of grains, the couple (a_{2k}, b_{2k}) cannot be the same as the couple (a_{2k-1}, b_{2k-1}). Thus, there are at least $N-2$ changes in the sequence of couples $\{(a_m, b_m)\}_{m=1}^{2N-4}$, which means that there are at least $(N-2)/2$ changes in at least one of the sequences $\{a_m\}$ and $\{b_m\}$.

Now form the subsequences $\{\hat{a}_m\}$ and $\{\hat{b}_m\}$ of the sequences $\{a_m\}$ and $\{b_m\}$ such that the elements repeated adjacently in the sequence $\{a_m\}$ and $\{b_m\}$ are represented only once in $\{\hat{a}_m\}$ and $\{\hat{b}_m\}$, respectively (see description of Fig. 3 (c)). Then from the previous paragraph it follows that at least one of the subsequences $\{\hat{a}_m\}$ and $\{\hat{b}_m\}$ has at least $(N-2)/2$ elements.

(6) Without loss of generality suppose that it is $\{\hat{a}_m\}$ whose length is bounded from below by $(N-1)/2$. If there exists a triple of indices $m_1 < m_2 < m_3$ such that $\hat{a}_{m_1} = x_i = \hat{a}_{m_3}$ and $\hat{a}_{m_2} = x_j$, $i \neq j$, then the boundaries ∂x_i and ∂x_j have to meet at least twice. Therefore, there cannot exist m_4 such that $a_{m_4} = x_j$, because in such case at least three intersections of ∂x_i and ∂x_j would occur and it is against the assumption (4) imposed on the grains. Therefore, the sequence satisfies the conditions

(a) for all $m = 1, 2, \dots$, we have $\hat{a}_m \neq \hat{a}_{m+1}$,

(b) there does not exist $s = 4$ indices $m_1 < m_3 < m_2 < m_4$ such that $a_{m_1} = a_{m_3} \neq a_{m_2} = a_{m_4}$.

Such a sequence is called a Davenport-Schinzel sequence of order s (briefly s-DS sequence, see [10]) and its properties are used in the remaining part of the proof.

(7) Denote by $\lambda_{s-2}(n)$ the maximal length of an s-DS sequence formed by n mutually different elements. Then it can be shown that $\lambda_s(n) = 2n-1$ (see [10]). Thus, when we have n different elements, we can form a 4-DS sequence with maximal length equal to $2n-1$ (see [10]). Since the length of the sequence $\{\hat{a}_m\}$ is at least $(N-2)/2 = \lambda_2(n) = 2n-1$, we need at least $n = N/4$ different elements of this sequence, i.e. at least $n = N/4$ different grains. Thus for n grains, the maximal number of holes is equal to $4n$. □

3.2. Attractiveness and repulsiveness. For theoretical results in this part as well as for the simulation described in the following section, Papangelou conditional intensity (see [6]) is an important term.

For a finite configuration $\mathbf{x}$ of the objects $\{x_1, \ldots, x_n\}$ and for an object $y \notin \mathbf{x}$, Papangelou conditional intensity is defined as

$$\lambda_{\boldsymbol{\theta}}(\mathbf{x}, y) = f_\theta(\mathbf{x} \cup y)/f_\theta(\mathbf{x}).$$

Denoting by

$$G(\mathbf{x}, y) = G(U_{\mathbf{x}} \cup y) - G(U_{\mathbf{x}})$$

the increment of an arbitrary geometrical characteristic $G \in \{A, L, \chi\}$ when adding an object y to the configuration $\mathbf{x}$, we get

$$\lambda_{\boldsymbol{\theta}}(\mathbf{x}, y) = \exp\{\theta_1 A(\mathbf{x}, y) + \theta_2 L(\mathbf{x}, y) + \theta_3 \chi(\mathbf{x}, y)\}. \tag{3.1}$$

It means that Papangelou conditional intensity $\lambda_{\boldsymbol{\theta}}(\mathbf{x}, y)$ depends only on the increments of the geometrical characteristics and not on the characteristics themselves nor on the normalizing constant. The proof of Proposition 3.3 below is based on this property.

The properties to be studied here are attractiveness and repulsiveness. They are defined as follows. The Quermass-interaction process with convex compact grains (2.1) is called

(1) attractive if $\lambda_{\boldsymbol{\theta}}(\mathbf{x}_1, y) \leqslant \lambda_{\boldsymbol{\theta}}(\mathbf{x}_2, y)$ for all configurations $\mathbf{x}_1$, $\mathbf{x}_2$ such that $\mathbf{x}_1 \subset \mathbf{x}_2$,
(2) repulsive if $\lambda_{\boldsymbol{\theta}}(\mathbf{x}_1, y) \geqslant \lambda_{\boldsymbol{\theta}}(\mathbf{x}_2, y)$ for all configurations $\mathbf{x}_1$, $\mathbf{x}_2$ such that $\mathbf{x}_1 \subset \mathbf{x}_2$.

Proposition 3.3. *For the Quermass-interaction process with convex compact grains* (2.1)*, the following assertions hold:*

(1) *The process with $\theta_2 = \theta_3 = 0$ and $\theta_1 \neq 0$, i.e. the A-interaction process, is attractive for $\theta_1 < 0$ and repulsive for $\theta_1 > 0$.*
(2) *The process with $\theta_1 = \theta_3 = 0$ and $\theta_2 \neq 0$, i.e. the L-interaction process, is*
   (a) *both attractive and repulsive, if $L(\mathbf{X}) = 0$,*
   (b) *attractive for $\theta_2 < 0$ and repulsive for $\theta_2 > 0$, if $A(\mathbf{X}) = 0$ and $P(L(\mathbf{X}) > 0) > 0$,*
   (c) *neither attractive nor repulsive, if $P(A(\mathbf{X}) > 0) > 0$.*
(3) *The process with $\theta_1 = \theta_2 = 0$ and $\theta_3 \neq 0$, i.e. the χ-interaction process, is*
   (a) *both attractive and repulsive, if $L(\mathbf{X}) = 0$,*
   (b) *neither attractive nor repulsive, if $P(L(\mathbf{X}) > 0) > 0$.*

P r o o f. From additivity of Minkowski functionals, we have

$$A(\mathbf{x}, y) = A(y) - A(y \cap U_{\mathbf{x}}), \tag{3.2}$$

$$L(\mathbf{x}, y) = L(y) - L(y \cap U_{\mathbf{x}}). \tag{3.3}$$

In the whole proof, we suppose that the configurations $\mathbf{x}_1$, $\mathbf{x}_2$ satisfy $\mathbf{x}_1 \subset \mathbf{x}_2$.

(1) Since $A(U_{\mathbf{x}_1}) \leqslant A(U_{\mathbf{x}_2})$, we have $A(y \cap U_{\mathbf{x}_1}) \leqslant A(y \cap U_{\mathbf{x}_2})$ and so from (3.2) we get $A(\mathbf{x}_1, y) \geqslant A(\mathbf{x}_2, y)$. Hence, from (3.1) we have $\lambda_{\boldsymbol{\theta}}(\mathbf{x}_1, y) \leqslant \lambda_{\boldsymbol{\theta}}(\mathbf{x}_2, y)$ for $\theta_1 < 0$ and $\lambda_{\boldsymbol{\theta}}(\mathbf{x}_1, y) \geqslant \lambda_{\boldsymbol{\theta}}(\mathbf{x}_2, y)$ for $\theta_1 > 0$.

(2) Due to (3.3), the properties of $L(\mathbf{x}, y)$ differ in the following three cases:

(a) The only convex compact planar random set satisfying $L(\mathbf{X}) = 0$ is a random point. In this case $L(\mathbf{x}, y) = 0$ for all configurations $\mathbf{x}$ and all objects y. Hence, from (3.1) we have $\lambda_{\boldsymbol{\theta}}(\mathbf{x}_1, y) = \lambda_{\boldsymbol{\theta}}(\mathbf{x}_2, y) = 1$.

(b) The only convex compact planar random set satisfying $A(\mathbf{X}) = 0$ and $L(\mathbf{X}) > 0$ is a random line segment. Then $L(U_{\mathbf{x}_1}) \leqslant L(U_{\mathbf{x}_2})$, i.e. $L(y \cap U_{\mathbf{x}_1}) \leqslant L(y \cap U_{\mathbf{x}_2})$ and so from (3.3) we get $L(\mathbf{x}_1, y) \geqslant L(\mathbf{x}_2, y)$. Therefore, $\lambda_{\boldsymbol{\theta}}(\mathbf{x}_1, y) \leqslant \lambda_{\boldsymbol{\theta}}(\mathbf{x}_2, y)$ for $\theta_2 < 0$ and $\lambda_{\boldsymbol{\theta}}(\mathbf{x}_1, y) \geqslant \lambda_{\boldsymbol{\theta}}(\mathbf{x}_2, y)$ for $\theta_2 > 0$.

(c) Consider two situations which lead to different inferences:

(i) $U_{\mathbf{x}_1} \cap y = \emptyset$ and $U_{\mathbf{x}_2} \cap y = y$. Then $L(\mathbf{x_1}, y) = L(y)$ and $L(\mathbf{x_2}, y) = L(y) - L(y \cap U_{\mathbf{x}_2}) = 0$, therefore $L(\mathbf{x_1}, y) > L(\mathbf{x_2}, y)$.

(ii) There exists a configuration $\mathbf{x}_1$ such that $U_{\mathbf{x_1}}$ contains a hole which can be covered by the object y and moreover $\partial y \subset U_{\mathbf{x}_1}$, where ∂y denotes the boundary of the object y. Denote by L_h the boundary of the hole in the set $U_{\mathbf{x}_1}$, then $L(\mathbf{x}_1, y) = L(y) - L(y \cap U_{\mathbf{x}_1}) = L(y) - (L(y) + L_h) = -L_h < 0$. If $U_{\mathbf{x_2}}$ is such that $y \subset U_{\mathbf{x_2}}$, then $L(\mathbf{x}_2, y) = 0$, therefore $L(\mathbf{x}_1, y) < L(\mathbf{x}_2, y)$.

This together with (3.1) implies that the process is neither attractive nor repulsive.

(3) Distinguish between the following two situations:

(a) For a point process (i.e. the process with $L(\mathbf{X}) = 0$), we have $\chi(x) = 1$ for all points x, i.e. $\chi(\mathbf{x}, y) = 1$ for all configurations $\mathbf{x}$ and all objects y. Hence, from (3.1) we have $\lambda_{\boldsymbol{\theta}}(\mathbf{x}_1, y) = \lambda_{\boldsymbol{\theta}}(\mathbf{x}_2, y) = \exp\{\theta_3\}$.

(b) Similarly to the above, consider two situations:

(i) $U_{\mathbf{x}_1}$ is one connected component without any hole, $U_{\mathbf{x}_2}$ consists of two connected components without any hole, $U_{\mathbf{x}_1} \cap y \neq \emptyset$ and $U_{\mathbf{x}_2} \cup y$ forms one connected component. Then $\chi(\mathbf{x}_1, y) = \chi(U_{\mathbf{x}_1} \cup y) - \chi(U_{\mathbf{x}_1}) = 1 - 1 = 0$ and $\chi(\mathbf{x}_2, y) = \chi(U_{\mathbf{x}_2} \cup y) - \chi(U_{\mathbf{x}_2}) = 1 - 2 = -1$, i.e. $\chi(\mathbf{x_1}, y) > \chi(\mathbf{x_2}, y)$.

(ii) $U_{\mathbf{x}_1}$ forms two connected components without any hole, $U_{\mathbf{x}_1} \cup y$ forms one connected component without any hole and $y \subset U_{\mathbf{x}_2}$. Then $\chi(\mathbf{x}_1, y) = \chi(U_{\mathbf{x}_1} \cup y) - \chi(U_{\mathbf{x}_1}) = 1 - 2 = -1$ and $\chi(\mathbf{x}_2, y) = \chi(U_{\mathbf{x}_2} \cup y) - \chi(U_{\mathbf{x}_2}) = \chi(U_{\mathbf{x}_2}) - \chi(U_{\mathbf{x}_2}) = 0$, i.e. $\chi(\mathbf{x_1}, y) < \chi(\mathbf{x_2}, y)$.

This implies that the process is neither attractive nor repulsive. □

Note that the process with $\theta_1 = \theta_2 = \theta_3 = 0$, i.e. the Boolean model, is both attractive and repulsive, because in (3.1) for all configurations $\mathbf{x}$ and all objects y, we have $\lambda_{\boldsymbol{\theta}}(\mathbf{x}, y) = \exp\{0 \cdot A(\mathbf{x}, y) + 0 \cdot L(\mathbf{x}, y) + 0 \cdot \chi(\mathbf{x}, y)\} = 1$.

4. Simulation

4.1. MCMC algorithm. For simulation of the process, we use the basic Metropolis-Hastings birth-death algorithm (see [14]). It works as follows.

(1) Start from an arbitrary configuration $\mathbf{x_0}$ and suppose that in the t-th iteration we have a configuration $\mathbf{x_t} = \{x_1, \dots, x_n\}$.
(2) In the $(t+1)$-st iteration:
   (a) with probability $1/2$, the proposal is $\mathbf{x_t} \cup \{x_{n+1}\}$ and
      (i) we accept the proposal with probability $\min\{1; H(\mathbf{x_t}, x_{n+1})\}$ and set $\mathbf{x_{t+1}} = \mathbf{x_t} \cup \{x_{n+1}\}$,
      (ii) else we set $\mathbf{x_{t+1}} = \mathbf{x_t}$,
   (b) else, the proposal is $\mathbf{x_t} \setminus \{x_i\}$, $i \in \{1, \dots, n\}$, and
      (i) we accept the proposal with probability $\min\{1; 1/H(\mathbf{x_t} \setminus \{x_i\}, x_i)\}$ and set $\mathbf{x_{t+1}} = \mathbf{x_t} \setminus \{x_i\}$,
      (ii) else we set $\mathbf{x_{t+1}} = \mathbf{x_t}$,

where $H(\mathbf{x}, y) = \lambda_{\boldsymbol{\theta}}(\mathbf{x}, y)|S|/(n+1)$ for any finite configuration $\mathbf{x} = \{x_1, \dots, x_n\}$ and an object $y \notin \mathbf{x}$.

In this procedure, we need to calculate Papangelou conditional intensity in each iteration, so it is necessary to optimize its calculation.

Recall that Papangelou conditional intensity $\lambda_{\boldsymbol{\theta}}(\mathbf{x}, y)$ given by (3.1) depends only on the increments of the geometrical characteristics and not on the characteristics themselves nor on the normalizing constant. It plays an important role in this simulation algorithm, because as mentioned in [12] and [13], the normalizing constant $c_{\boldsymbol{\theta}}$ has no explicit form, its approximation is time-consuming and moreover, it need not be precise enough.

The second advantage which follows from the relation (3.1) is that the work with the increments instead of the whole characteristics allows us to make only local calculations and so to make the calculations faster. For example in [12], the power tessellation (also called the Laguerre tessellation, see e.g. [1]) of the union of discs was used. The power tessellation divides the union of the discs to the union of convex compact sets (so-called cells)

$$B_i = \{v \in U_{\mathbf{x}} \colon \|v - u_i\|^2 - r_i^2 < \|v - u_j\|^2 - r_j^2 \ \forall\, j \neq i\}$$

corresponding to the discs x_i with centres u_i and radii r_i, $i = 1, \ldots, n$. It holds almost surely that at most three of the cells meet at one point and then instead of the inclusion-exclusion formula

$$G(\mathcal{U}_{\mathbf{x}}) = \sum_i G(x_i) - \sum_{\{i_1,i_2\}} G(x_{i_1} \cap x_{i_2}) + \ldots + (-1)^{n+1} \sum_{\{i_1,\ldots,i_n\}} G(x_{i_1} \cap \ldots \cap x_{i_n})$$

for all geometrical characteristics $G \in \{A, L, \chi\}$, we can use

$$A(U_{\mathbf{x}}) = \sum_i A(B_i), \quad L(U_{\mathbf{x}}) = \sum_i L(B_i), \quad \chi(U_{\mathbf{x}}) = N_1 - N_2 + N_3,$$

where $L(B_i)$ is the length of the part of the boundary of B_i lying on the boundary of the set $U_{\mathbf{x}}$, N_1 is the number of nonempty cells in the tessellation, N_2 the number of interior edges (i.e. the boundaries between two cells) and N_3 the number of interior vertices (i.e. the intersections of three cells) in the tessellation. It allows to do only local calculations in the sense that when a disc is added or deleted, the geometrical characteristics are changed only through the cells intersected by this disc. These local calculations make the calculation of $\lambda_{\boldsymbol{\theta}}(\mathbf{x}, y)$ and consequently the usage of the MCMC algorithm significantly faster. Moreover, the calculation of the geometrical characteristics is easy. For example, due to the convexity of the cells, the area of each cell can be divided into the areas of triangles and disc caps, see [12].

The aim of the research presented here is to find some local calculations also for Quermass-interaction process with non circular grains. Unfortunately, it is difficult to use some analogy to the power tessellation, since the objects are realizations of a quite general random set $\mathbf{X}$. In the special case when we consider the random set $\mathbf{X}$ to be an ellipse with random axes, we can use a generalization of the Laguerre tessellation described in [1] such that the cells corresponding to the ellipses x_i with centres u_i, $i = 1, \ldots, n$, are defined as

$$B_i = \{v \in U_{\mathbf{x}} \colon\ d(v, u_i) < d(v, u_i)\ \forall\, j \neq i\},$$

where $d(v, u_i) = (v - u_i)^{\mathrm{T}} M_i (v - u_i)$ and M_i is a symmetric positive definite matrix such that its eigenvectors define the elliptical axes and the eigenvectors define their length. But since the cells are not convex, it does not allow us to work with the tessellation in the same way as in the case of the random disc process. It is impossible to calculate the cell area in the way mentioned above and the calculation of the remaining characteristic is more complicated as well.

Therefore, we found another way of local calculations. It is based on discretization of the set described in the neet section.

4.2. Discretization. For calculation of geometrical characteristics in (2.1) and (3.1), we use a discretization where the needed values are kept in cells (or pixels) of a chosen grid. In each cell of the grid, we have the information about

- ▷ the area of the cell,
- ▷ the perimeter by which the cell contributes to the perimeter of the union,
- ▷ the neighborhood of the pixel needed for using the classical algorithm for calculation of the Euler-Poincaré characteristic based on local patterns (see below),
- ▷ list of objects overlapping the cell

as illustrated in Fig. 4. Then in the case when an object is added or deleted, the geometrical characteristics are recalculated only in the cells overlapped by this object.

4.2.1. Calculation of the area. The area of the cell is always 0 or 1 pixel, depending on whether the corresponding cell belongs to the analyzed set or not. For this notification, we use the planar coordinates of the centre of the cell. When we consider the cell $[k,l] = \langle a, a+\Delta\rangle \times \langle b, b+\Delta\rangle$, we simply calculate whether the point $(a+\Delta/2, b+\Delta/2)$ belongs to x, where x is the recently added or deleted object.

4.2.2. Calculation of the perimeter. There are many publications concerning calculation of the perimeter of sets displayed in digital image. For example in [16], the perimeter is estimated by intrinsic volume densities using the Steiner formula, the authors of [17] estimate the perimeter using the Cauchy formula, etc. Many of these methods work with the whole digital image in order to make the estimation precise enough. But our main aim is to make the calculations as local as possible rather than to achieve the absolute precision, so we need to apply an easy algorithm, where the inputs are close neighbourhoods of pixels belonging to the actually added or deleted object.

Let "1" denote the pixel belonging to the analyzed set and "0" the pixel not belonging to the analyzed set. In order to calculate the perimeter by which the cell contributes to the perimeter of the union in our case, we focus just on the nearest neighbouring cells. For a pixel $[k,l]$ belonging to the analyzed set denote the six different types of situations due to the neighbouring pixels by $[k,l-1]$, $[k,l+1]$, $[k-1,l]$, and $[k+1,l]$ as

$\mathbf{P_0}$:

	1	
1	1	1
	1	

$\mathbf{P_1}$:

	0	
1	1	1
	1	

	1	
1	1	0
	1	

	1	
1	1	1
	0	

	1	
0	1	1
	1	

$\mathbf{P_{2a}}$:

	0	
1	1	0
	1	

	1	
1	1	0
	0	

	1	
0	1	1
	0	

	0	
0	1	1
	1	

$\mathbf{P_{2b}}$:

	0	
1	1	1
	0	

	1	
0	1	0
	1	

$\mathbf{P_3}$:

	0	
1	1	0
	0	

	1	
0	1	0
	0	

	0	
0	1	1
	0	

	0	
0	1	0
	1	

$\mathbf{P_4}$:

	0	
0	1	0
	0	

Then the pixels contribute to the whole perimeter by the following values:

(1) The contribution of each pixel not belonging to the analyzed set is 0.
(2) The contribution of a pixel belonging to the analyzed set is
   (a) 0 for the type $\mathbf{P_0}$,
   (b) 1 for the type $\mathbf{P_1}$,
   (c) $\sqrt{2}$ for the type $\mathbf{P_{2a}}$,
   (d) 2 for the type $\mathbf{P_{2b}}$,
   (e) 3 for the type $\mathbf{P_3}$,
   (f) 4 for the type $\mathbf{P_4}$.

4.2.3. Calculation of the Euler-Poincaré characteristic. For calculation of the Euler-Poincaré characteristic, we use a simple algorithm based on local (2×2)-pixel patterns (see e.g. [18]). Consider three types of such patterns, namely

$\mathbf{Q_1}$:

1	0
0	0

0	1
0	0

0	0
1	0

0	0
0	1

$\mathbf{Q_2}$:

1	1
1	0

1	1
0	1

1	0
1	1

0	1
1	1

$\mathbf{Q_3}$:

1	0
0	1

0	1
1	0

For $i = 1, 2, 3$ denote by $n(\mathbf{Q}_i)$ the number of the patterns of the type $\mathbf{Q_i}$ in the digital image of the given set. Then the Euler-Poincaré characteristic of the set is calculated as

$$\chi = \frac{1}{4}(n(\mathbf{Q}_1) - n(\mathbf{Q}_2) + 2n(\mathbf{Q}_3))$$

under the definition of four-connectivity and

$$\chi = \frac{1}{4}(n(\mathbf{Q}_1) - n(\mathbf{Q}_2) - 2n(\mathbf{Q}_3))$$

for eight-connectivity. In our simulation study below, we use the definition of four-connectivity and the information about the type of 2×2 pattern is obtained in the "upper left" pixel, i.e. the type of the pixel $[k, l]$ is the type of the pattern

$[k, l]$	$[k, l+1]$
$[k+1, l]$	$[k+1, l+1]$

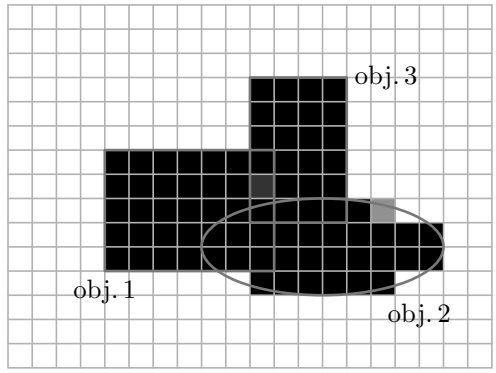

Figure 4. An example of the grid, where the light grey cell has area = 1, perimeter = $\sqrt{2}$, type = $\mathbf{Q_2}$, list of objects = $\{2\}$ and the dark grey cell has area = 1, perimeter = 0, type = $-$ (i.e. it is not used for calculation of Euler-Poincaré characteristic), list of objects = $\{1, 3\}$.

4.3. Examples.

4.3.1. Rectangles and ellipses. In the first example, we consider the primary grain $\mathbf{X}$ to be either a rectangle or an ellipse, so the probability distribution Q of $\mathbf{X}$ is given by

$$Q = \alpha Q^{(\mathrm{rect})} + (1 - \alpha)Q^{(\mathrm{el})}, \tag{4.1}$$

where $\alpha \in (0, 1)$ and both $Q^{(\mathrm{rect})}$ and $Q^{(\mathrm{el})}$ are determined by two random parameters $A^{(\mathrm{rect})}$, $B^{(\mathrm{rect})}$ and $A^{(\mathrm{el})}$, $B^{(\mathrm{el})}$, respectively. It means that

$$\mathbf{X} = \mathbb{I}_{\{K \leqslant \alpha\}}\mathbf{X}_1 + \mathbb{I}_{\{K > \alpha\}}\mathbf{X}_2,$$

where

$$\mathbf{X}_1 = (-A^{(\mathrm{rect})}/2, A^{(\mathrm{rect})}/2) \times (-B^{(\mathrm{rect})}/2, B^{(\mathrm{rect})}/2),$$
$$\mathbf{X}_2 = \{(x, y)\colon\ (x/A^{(\mathrm{el})})^2 + (y/B^{(\mathrm{el})})^2 \leqslant 1\},$$

and $K \sim U(0, 1)$ is a random variable independent of $\mathbf{X}_1$ and $\mathbf{X}_2$.

In this example, we consider the reference Boolean model with intensity $\varrho = 1$ in $S = [0, 10] \times [0, 10]$ and the distribution Q of $\mathbf{X}$ given by $\alpha = 0.3$, $A^{(\mathrm{rect})} \sim U(0.2, 1.2)$, $B^{(\mathrm{rect})} \sim U(0.2, 0.7)$, $A^{(\mathrm{el})} \sim U(0.2, 0.5)$, and $B^{(\mathrm{el})} \sim U(0.2, 0.7)$, where all these random variables are mutually independent, see Fig. 5 (a). Simulated realizations of Quermass-interaction process with non circular grains with different parameters are shown in Fig. 5 (b)–(d). In this figure, we observe that for negative θ_1 and positive θ_2 (images (b) and (c)), i.e. when the realizations with smaller area and larger perimeters are preferred, we have more rugged images compared to the reference process (a), while in the image (b), where θ_3 is positive, i.e., larger Euler-Poincaré characteristic is preferred, we can see more of smaller components and in the image (c) for θ_3 negative, we have less of protracted components. When we set θ_1 to be positive and θ_2 to be negative, the realizations tend to produce patterns as seen in the image (d) while θ_3 negative causes occurrence of a number of holes.

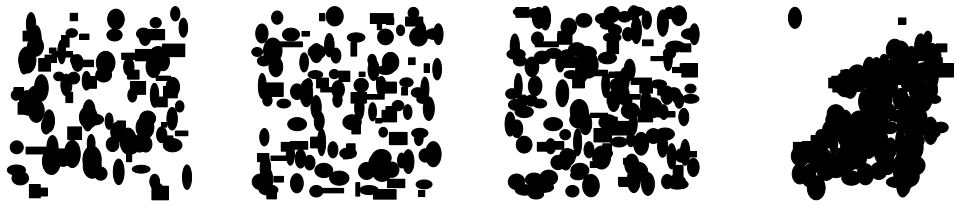

(a) (b) (c) (d)

Figure 5. Realizations of (a) the reference Boolean model on $S = [0, 10] \times [0, 10]$ with intensity $\varrho = 1$ and the distribution given by (4.1) with $\alpha = 0.3$, $A^{(\mathrm{rect})} \sim U(0.2, 1.2)$, $B^{(\mathrm{rect})} \sim U(0.2, 0.7)$, $A^{(\mathrm{el})} \sim U(0.2, 0.5)$ and $B^{(\mathrm{el})} \sim U(0.2, 0.7)$, (b) (A, L, χ)-interaction model with parameters $(\theta_1, \theta_2, \theta_3) = (-4, 1, 0.5)$, (c) (A, L, χ)-interaction model with parameters $(\theta_1, \theta_2, \theta_3) = (-4, 1, -0.5)$ and (d) (A, L, χ)-interaction model with parameters $(\theta_1, \theta_2, \theta_3) = (3, -1.5, -1.5)$.

4.3.2. Rotated ellipses. In the second example $\mathbf{X}$ is a rotated ellipse, where both the lengths A, B and the angle φ of its rotation are random.

The reference Boolean model is again considered with intensity $\varrho = 1$ in $S = [0, 10] \times [0, 10]$, and the distribution Q of $\mathbf{X}$ is given by $A \sim U(0.4, 0.7)$, $B \sim U(0.2, 0.4)$ and $\varphi \sim U(\pi/8, 3\pi/8)$, i.e. the direction of the main axes of the ellipses are not distributed uniformly at all possible angles, but the ellipses are inclined, see Fig. 6 (a). Simulated realizations of Quermass-interaction process with elliptical

grains with different parameters is shown in Fig. 6 (b)–(d). Similarly to the above, we observe that for negative θ_1 and positive θ_2 (images (b) and (c)) the images are more rugged compared to the reference process (a), while in the image (b), where θ_3 is positive, we have more of smaller components and in the image (c) for θ_3 negative we observe protracted clusters. Another type of clustering is observed in the image (d). There we set θ_1 to be positive, θ_2 to be negative, which forces the realization to produce rather circular clusters while θ_3 positive causes occurrence of a larger number of such clusters.

(a) (b) (c) (d)

Figure 6. Realizations of (a) the reference Boolean model on $S = [0, 10] \times [0, 10]$ with intensity $\varrho = 1$ and the parameters $A \sim U(0.2, 0.4)$, $B \sim U(0.4, 0.7)$ and $\varphi \sim U(\pi/8, 3\pi/8)$,
(b) (A, L, χ)-interaction model with parameters $(\theta_1, \theta_2, \theta_3) = (-3, 1, 1)$,
(c) (A, L, χ)-interaction model with parameters $(\theta_1, \theta_2, \theta_3) = (-3, 1, -0.5)$ and
(d) (A, L, χ)-interaction model with parameters $(\theta_1, \theta_2, \theta_3) = (3, -1, 2)$.

4.4. Comparison to simulation of random disc process using power tessellation. We are naturally interested also in comparison of the simulations of random disc Quermass-interaction process by the method described in [12] using the power tessellation and by the method using discretization described in this paper. Two main questions surely are:

(1) How much similar the simulated realizations are?
(2) Which method is faster and how much?

Of course, the answers depend on the chosen resolution of the used discretization. By refining the grid, we achieve more precise results, but the simulation time quadratically grows. It is not possible to recommend a concrete refinement in general, because it depends on many aspects of the studied situation, mainly on the size of the window S and the distribution of the grains. However, let us provide at least a short simulation study in order to compare these two methods in one concrete case.

Consider the reference random disc Boolean model with disc centres in $S = [0, 10] \times [0, 10]$, intensity of the centres $\varrho = 1$ and the distribution of the radii $U(0.2, 0.6)$.

First, we simulate the process with $(\theta_1, \theta_2, \theta_3) = (-3, 1, -1.5)$ producing realizations with long connected components in which the influence of the resolution can

be significant. In Fig. 7, we observe the realizations obtained by discretization with the resolutions (b) 100×100, (c) 300×300 and (d) 500×500 pixels (imaged both as smooth discs and in the corresponding resolution) compared to (a) the realization obtained by the simulation using the power tessellation algorithm. We can see that in the case of quite rough resolution 100×100, the realization is not very similar to the realization (a). It can be caused by the fact, that for small discs and rough resolution, the perimeter is overvalued and since the process with given parameters prefers larger perimeter, it produces more discs. In the case of smoother resolution, we observe much better results, and also in their pixel image we observe almost circular shapes of the discs. However, when we compare the time needed for the simulation, it is approximately 4× longer for the resolution 100×100 (i.e. 36× longer for the resolution 300×300 and 100× longer for the resolution 500×500) than for the simulation using the power tessellation algorithm.

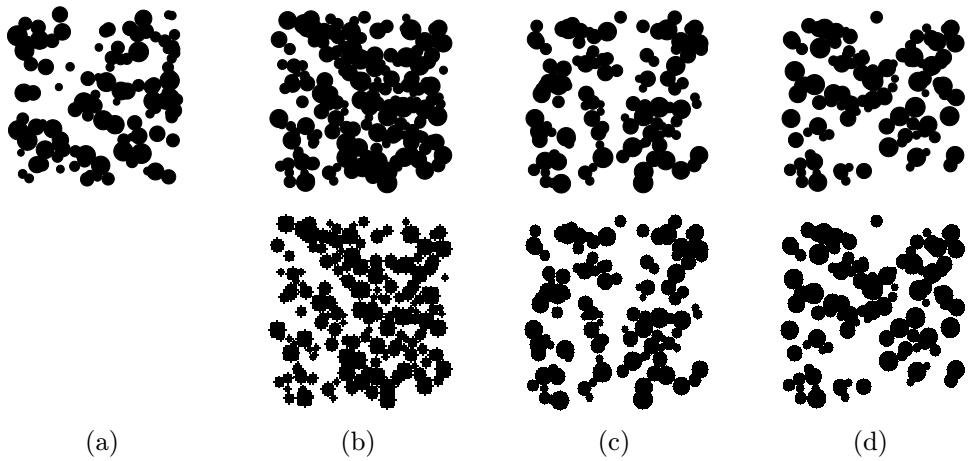

(a) (b) (c) (d)

Figure 7. Realizations of random disc Quermass-interaction process with the reference Boolean model on $S = [0, 10] \times [0, 10]$ with intensity $\varrho = 1$, the distribution of the radii $U(0.2, 0.6)$ and $(\theta_1, \theta_2, \theta_3) = (-3, 1, -1.5)$ obtained by the simulation using the power tessellation algorithm (a) and by the simulation using the discretization algorithm, where the resolution is (b) 100×100, (c) 300×300 and (d) 500×500 pixels. The first row is the image of the discs themselves, the second row are the same realizations plotting the corresponding resolution.

Secondly, we fix the resolution 400×400 and study other combinations of parameters. In Fig. 8 in the cases (a) and (b), we set θ_1 to be negative, θ_2 to be positive and θ_3 to be negative, i.e. we expect the realizations with rather greater number of small components. Both the images are similar, only in the image (a) we observe slightly less area. For θ_1 positive, θ_2 as well as θ_3 negative as chosen in cases (c) and (d), where the realizations are big clusters with holes, the similarity is obvious again.

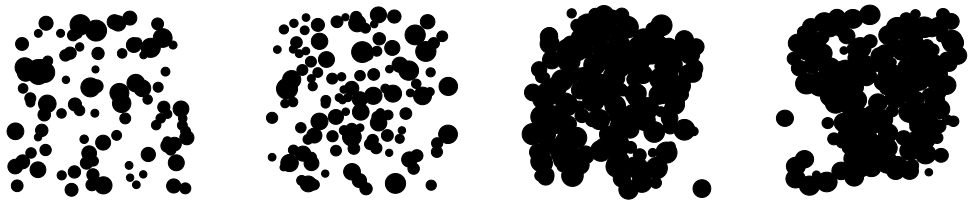

(a) (b) (c) (d)

Figure 8. Realizations of random disc Quermass-interaction process with the reference Boolean model on $S = [0, 10] \times [0, 10]$ with intensity $\varrho = 1$ and the distribution of the radii $U(0.2, 0.6)$, where (a) $(\theta_1, \theta_2, \theta_3) = (-4, 1, -0.5)$ and the simulation used the power tessellation algorithm, (b) $(\theta_1, \theta_2, \theta_3) = (-4, 1, -0.5)$ and the simulation used the discretization algorithm, (c) $(\theta_1, \theta_2, \theta_3) = (1.2, -1, -1)$ and the simulation used the power tessellation algorithm, and (d) $(\theta_1, \theta_2, \theta_3) = (1.2, -1, -1)$ and the simulation used the power discretization algorithm.

5. Conclusion

In this paper, we generalized the random disc Quermass-interaction model to the process of interacting convex compact grains. After deriving theoretical results, we focused on simulation of the process. The simulation algorithm used local calculations in order to run faster, similarly to [12], where the power tessellation of the union of discs was introduced. A similar tool was not found in the case of general convex compact grains, therefore instead of it, we worked with a discretization of the window in which the process is analyzed. It entailed the problem of choosing the grid of the discretization. As shown in the last section, the grid must be chosen carefully, because in case of a very coarse grid, the simulation is quite fast, but the preciseness is not satisfactory, and vice versa. But despite the introduced problems, the conclusion is that we provided a satisfactory simulation algorithm, which can be later used for further analyses.

References

[1] *H. Altendorf, F. Latourte, D. Jeulin, M. Faessel, L. Saintyant*: 3D reconstruction of a multiscale microstructure by anisotropic tessellation models. Image Anal. Stereol. *33* (2014), 121–130.

[2] *S. N. Chiu, D. Stoyan, W. S. Kendall, J. Mecke*: Stochastic Geometry and Its Applications. Wiley Series in Probability and Statistics, John Wiley & Sons, Chichester, 2013.

[3] *D. Dereudre*: Existence of Quermass processes for non locally stable interaction and non bounded convex grains. Adv. Appl. Probab. *41* (2009), 664–681.

[4] *D. Dereudre, F. Lavancier, K. Staňková Helisová*: Estimation of the intensity parameter of the germ-grain Quermass-interaction model when the number of germs is not observed. Scand. J. Stat. *41* (2014), 809–829.

[5] *P. J. Diggle*: Binary mosaics and the spatial pattern of heather. Biometrics *37* (1981), 531–539.

[6] *C. J. Geyer, J. Møller*: Simulation procedures and likelihood inference for spatial point processes. Scand. J. Stat. *21* (1994), 359–373.
[7] *K. Helisová*: Modeling, statistical analyses and simulations of random items and behavior on material surfaces. Supplemental UE: TMS 2014 Conference Proceedings, San Diego, 2014, pp. 461–468.
[8] *P. Hermann, T. Mrkvička, T. Mattfeldt, M. Minárová, K. Helisová, O. Nicolis, F. Wartner, M. Stehlík*: Fractal and stochastic geometry inference for breast cancer: a case study with random fractal models and Quermass-interaction process. Stat. Med. *34* (2015), 2636–2661.
[9] *W. S. Kendall, M. N. M. van Lieshout, A. J. Baddeley*: Quermass-interaction processes: conditions for stability. Adv. Appl. Probab. *31* (1999), 315–342.
[10] *M. Klazar*: Generalised Davenport-Schinzel sequences: results, problems and applications. Integers: The Electronic Journal of Combinatorial Number Theory *2* (2002), A11.
[11] *I. Molchanov*: Theory of Random Sets. Probability and Its Applications, Springer, London, 2005.
[12] *J. Møller, K. Helisová*: Power diagrams and interaction processes for unions of discs. Adv. Appl. Probab. *40* (2008), 321–347.
[13] *J. Møller, K. Helisová*: Likelihood inference for unions of interacting discs. Scand. J. Stat. *37* (2010), 365–381.
[14] *J. Møller, R. P. Waagepetersen*: Statistical Inference and Simulation for Spatial Point Processes. Monographs on Statistics and Applied Probability 100, Chapman and Hall/CRC, Boca Raton, 2004.
[15] *T. Mrkvička, T. Mattfeldt*: Testing histological images of mammary tissues on compatibility with the Boolean model of random sets. Image Anal. Stereol. *30* (2011), 11–18.
[16] *T. Mrkvička, J. Rataj*: On the estimation of intrinsic volume densities of stationary random closed sets. Stochastic Processes Appl. *118* (2008), 213–231.
[17] *J. Ohser, F. Mücklich*: Statistical Analysis of Microstructures in Materials Science. Wiley Series in Statistics in Practice, Wiley, Chichester, 2000.
[18] *W. K. Pratt*: Digital Image Processing. Wiley & Sons, New York, 2001.
[19] *R Development Core Team*: R: A language and environment for statistical computing. R Found Stat Comp, Vienna. `http://www.R-project.org/`, 2010.
[20] *K. Staňková Helisová, J. Staněk*: Dimension reduction in extended Quermass-interaction process. Methodol. Comput. Appl. Probab. *16* (2014), 355–368.
[21] *M. Zikmundová, K. Staňková Helisová, V. Beneš*: Spatio-temporal model for a random set given by a union of interacting discs. Methodol. Comput. Appl. Probab. *14* (2012), 883–894.
[22] *M. Zikmundová, K. Staňková Helisová, V. Beneš*: On the use of particle Markov chain Monte Carlo in parameter estimation of space-time interacting discs. Methodol. Comput. Appl. Probab. *16* (2014), 451–463.

Authors' addresses: *Kateřina Helisová*, Czech Technical University in Prague, Faculty of Electrical Engineering Department of Mathematics, Technická 2, 166 27 Praha 6, Czech Republic, e-mail: `helisova@math.feld.cvut.cz`; *Jakub Staněk*, Department of Mathematics Education, Charles University, Sokolovská 83, 186 75 Praha 8, Czech Republic, e-mail: `stanekj@karlin.mff.cuni.cz`.